

Acoustic-mode vibrational anharmonicity in Cr-Si alloy single crystals

A. R. E. Prinsloo, H. L. Alberts, and P. Smit

Department of Physics, Rand Afrikaans University, P.O. Box 524, Auckland Park 2006, Johannesburg, South Africa

(Received 2 May 1997)

Measurements are reported of the hydrostatic-pressure dependences of the elastic constants of Cr+0.5 at. % Si and Cr+1.6 at. % Si alloy single crystals through the Néel transition. In the former crystal the Néel transition is a second-order incommensurate (I) spin-density-wave (SDW)-to-paramagnetic (P) transition, while it is a first-order commensurate (C) SDW-to-P transition in the latter crystal. The pressure derivatives of the elastic constants at different constant temperatures are used to calculate the acoustic-mode Grüneisen parameters, which quantify the vibrational anharmonicity, as a function of temperature through the Néel transition of each crystal. For the Cr+0.5 at. % Si crystal the mean long-wavelength acoustic mode Grüneisen parameter, $\bar{\gamma}^{e'l} \approx -5$, jumps by $\Delta \bar{\gamma}^{e'l} = 30$, from $\bar{\gamma}^{e'l} \approx -5$ to $\bar{\gamma}^{e'l} = +25$, in going through the second-order ISDW-P Néel transition, and then decreases to a value of $\bar{\gamma}^{e'l} \approx +5$ at temperatures well into the paramagnetic phase. This jump is much larger, $\Delta \bar{\gamma}^{e'l} = 170$, from $\bar{\gamma}^{e'l} = -50$ to $\bar{\gamma}^{e'l} = +150$, in going through the first-order CSDW-P Néel transition of Cr+1.6 at. % Si, after which $\bar{\gamma}^{e'l}$ decreases to $\bar{\gamma}^{e'l} \approx 0$ at temperatures deep into the paramagnetic phase. The results show very strong coupling of the SDW to the long-wavelength longitudinal-acoustic phonons in both crystals. Coupling to the long-wavelength shear acoustic phonons is relatively weak. In both crystals there is also strong coupling of the longitudinal phonons with the spin fluctuations above T_N . The present measurements are compared with anharmonic effects observed through the second-order CSDW-P Néel transitions of Cr+0.3 at. % Ru and Cr+3.5 at. % Al alloy single crystals. [S0163-1829(97)00342-1]

I. INTRODUCTION

Nonlinear acoustic properties of antiferromagnetic Cr alloys are presently receiving attention in the literature.¹⁻³ Experimental studies of the vibrational anharmonicity were reported for Cr+0.3 at. % Ru (Refs. 1 and 2) and Cr+3.5 at. % Al (Ref. 3) dilute alloy single crystals through the incommensurate (I)-to-commensurate (C) spin-density-wave (SDW) magnetic phase transition of the former crystal and through the CSDW-paramagnetic phase (P) Néel transitions of both. Unusual behavior was found for the anharmonicity in the SDW phases of these two alloys. The anharmonicity is quantified by the acoustic-mode Grüneisen parameters which give information on the interaction of the acoustic phonons with the SDW as well as on the role of volume and shear strains in the different magnetic phase transitions in the alloys. The long-wavelength acoustic Grüneisen parameter (γ_p) was found^{1,2} to be large and negative, which is unusual, in the CSDW and ISDW phases of Cr+3.0 at. % Ru, with γ_p being substantially larger negative for the CSDW than for the ISDW phase. γ_p for the CSDW phase of Cr+3.5 at. % Al is³ also negative and jumps to a very large positive value just above the Néel temperature (T_N), which is also unusual and not expected for the paramagnetic phase.⁴ On the other hand, the shear acoustic-mode Grüneisen parameters for [100] propagation behaves normally for both alloys, being small and positive like that⁴ for a Cr+5 at. % V alloy which remains paramagnetic at all temperatures above 0 K, and are only slightly affected by the different magnetic phase transitions. In both Cr+0.3 at. % Ru and Cr+3.5 at. % Al the SDW was found¹⁻³ to couple strongly with the longitudinal-mode acoustic phonons. Coupling with the shear-mode acoustic phonons is relatively weak. Nonlinear acoustic properties have not yet been studied for dilute Cr-Si alloys.

These alloys are of interest as they form together with Cr-Fe alloys, the only Cr systems that show^{5,6} first-order CSDW-P Néel transitions, in contrast with Cr-Ru and Cr-Al alloys, for which this transition is a second-order one. It should therefore be of interest to study the nonlinear acoustic properties of a Cr-Si alloy through the Néel transition. Also of interest is a study of these properties for a Cr alloy through an ISDW-P Néel transition. This was not done before since the only two alloys studied up to now, Cr+0.3 at. % Ru and Cr+3.5 at. % Al, both show CSDW-P Néel transitions. The magnetic phase diagram of the Cr-Si alloy system contains a triple point concentration (c_t) where the CSDW, ISDW, and P phases coexist. For concentrations $c < c_t$ the Néel transition is a second-order ISDW-P transition and for $c > c_t$ it is a first-order CSDW-P one.⁷ The Cr-Si system is thus ideally suited for studies of anharmonic effects through both a first-order CSDW-P and a second-order ISDW-P Néel transition, depending on the alloy concentration chosen.

In the present work a detailed study of anharmonic effects as a function of temperature, is reported for two dilute Cr-Si alloy single crystals, containing, respectively, 0.5 and 1.6 at. % Si. For the former crystal $c < c_t$ and the Néel transition is a second-order ISDW-P transition, while for the latter $c > c_t$, giving a first-order CSDW-P transition.

II. EXPERIMENTAL METHODS

The two crystals used in the present study are the same ones previously⁸ used for measurements of the temperature dependence of the elastic constants at atmospheric pressure. The preparation of the crystals was previously⁸ described. As the acoustic-mode Grüneisen parameters of a crystal are obtained from measurements of the pressure dependences of the second-order elastic constants, we measured the elastic

constants of the Cr+0.5 at. % Si and Cr+1.6 at. % Si alloy single crystals as a function of applied pressure at different constant temperatures through T_N . Elastic constants were obtained from ultrasonic (10 MHz) wave velocity measurements in the [100] and [110] propagation directions. The data at atmospheric pressure were previously⁸ reported. Standard pulse-echo overlap ultrasonic techniques⁹ were used for wave velocity measurements. Velocity data were corrected for transducer diffraction effects by using methods developed by Kittinger.¹⁰ The sensitivity of the measuring technique was 1 part in 10^5 and the error in the absolute values of the sound velocity is about 0.5%. Hydrostatic pressure in the range of 0–0.16 GPa was generated by a high-pressure gas system using nitrogen gas as the pressure medium. Pressure measurements were done at constant fixed temperatures in the temperature range 230–380 K. The temperatures were kept constant to within 0.2 K or better during pressure runs. At the lowest temperatures (about 230 K) the maximum available pressures were restricted to about 40×10^6 to 60×10^6 Pa, due to leaks occurring in the system above these pressures at the lowest temperatures. At room temperature and above, 0.16 GPa was attainable. Velocity measurements were also done on the Cr+0.5 at. % Si alloy as a function of temperature at different constant fixed pressures in order to determine the pressure dependence of the Néel temperature (T_N). In this case pressure could be kept constant to better than 10^{-3} GPa during the temperature runs.

III. HYDROSTATIC PRESSURE DERIVATIVES OF THE SECOND-ORDER ELASTIC CONSTANTS

The pressure derivatives of the second-order adiabatic elastic constants, c_{ij} , were determined from the ultrasonic wave velocity measurements as a function of pressure for each propagation mode, by using the equation

$$\left(\frac{\partial c_{ij}}{\partial P}\right)_{P=0} = (c_{ij})_{P=0} \left[2 \frac{\partial W / \partial P}{W} + \frac{1}{3B} \right]_{P=0}. \quad (1)$$

Here W is the natural velocity, defined¹¹ as the path length at zero pressure divided by the transit time at pressure P .

Due to the large ultrasonic attenuation in the CSDW phase for the c_{11} propagation mode,⁸ we obtained $[dc_{ij}/dP]_{P=0}$ for both crystals only from [110] wave propagation measurements. This means that the experimental error in $[dc_{11}/dP]_{P=0}$, calculated from the sums and differences between the measured values of $[dc_L/dP]_{P=0}$, $[dc_{44}/dP]_{P=0}$, and $[dc'/dP]_{P=0}$, is larger than that in the last mentioned three quantities. Here $c_L = \frac{1}{2}(c_{11} + c_{12} + 2c_{44})$ and $c' = \frac{1}{2}(c_{11} - c_{12})$.

The Néel temperature of Cr+0.5 at. % Si is 278 K and for Cr+1.6 at. % Si it is 253 K on heating and 245 K on cooling.⁸ The different T_N values for the latter crystal stem from the first-order nature of its Néel transition. High-pressure ultrasonic wave velocity measurements were done at ten different constant temperatures for Cr+0.5 at. % Si in the temperature range 240 to 380 K and at ten different temperatures for Cr+1.6 at. % Si in the temperature range 230–380 K. For both crystals these temperature ranges include the Néel point. To save space we will only show representative results for the longitudinal wave propagation mode of the

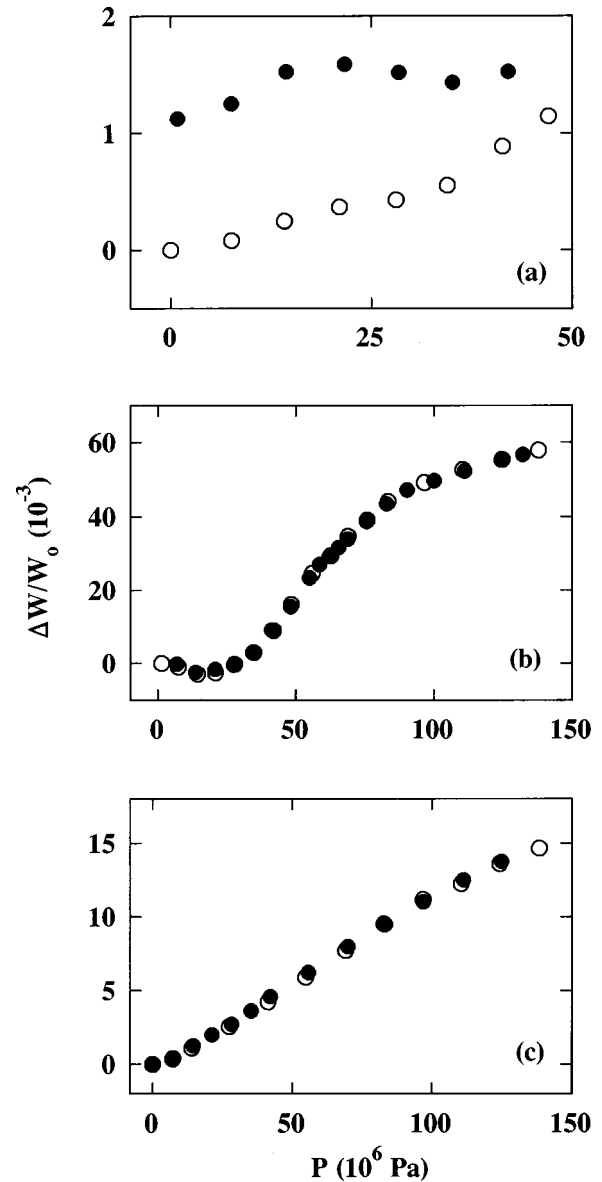


FIG. 1. Pressure dependence of the relative change in natural velocity, $\Delta W/W_0$, for the c_L mode of Cr+0.5 at. % Si at (a) $T = 250$ K, (b) $T = 275$ K and (c) $T = 331$ K. In (a), (b), and (c) \circ represents the results for increasing and \bullet for decreasing pressure. Note the different pressure scales.

Cr+0.5 at. % Si crystal and only at three of the above temperatures; at a temperature below T_N , close to T_N and one above T_N . We will furthermore not show the data for the shear propagation modes, the c_{44} and c' modes, of this crystal graphically, but will only discuss the observations for these modes qualitatively. Figure 1 shows the pressure dependence of $\Delta W/W_0$ for the longitudinal wave propagation mode at constant temperatures of, respectively, 250, 275, and 331 K for the Cr+0.5 at. % Si crystal. Here $\Delta W/W_0 = W_P/W_0 - 1$, where W_0 is the natural velocity at $P=0$ and W_P is that at pressure P . The interesting features of the pressure behavior of $\Delta W/W_0$ are:

(1) For all temperatures studied well below T_N , $\Delta W/W_0$ for the c_L longitudinal wave propagation mode changes only slightly with pressure and the change is hysteretic [Fig. 1(a) as an example]. At a temperature $T < T_N$, but close to T_N ,

the change in $\Delta W/W_0$ with pressure for the c_L propagation mode decreases slowly at first up to a critical pressure, after which it increases very rapidly on further increasing of pressure [Fig. 1(b)]. There are no hysteresis effects. This behavior is ascribed to the ISDW-P transition being induced by the critical pressure. At all temperatures studied above T_N , $\Delta W/W_0$ for the c_L propagation mode changes relatively rapidly and approximately linearly with pressure, without any hysteresis effects [Fig. 1(c) as an example]. The slope of these $\Delta W/W_0 - P$ curves at $T > T_N$ is very large close to T_N [$\approx 1.8 \text{ (GPa)}^{-1}$ at $T = 256 \text{ K}$] and decreases on further increasing the temperature to above T_N [$\approx 0.03 \text{ (GPa)}^{-1}$ at $T = 279 \text{ K}$]. The pressure behavior of $\Delta W/W_0$ of the c_L mode is anomalous at all temperatures. For a normal paramagnetic material, like for instance a Cr+5 at. % V alloy that is taken¹² to represent the nonmagnetic state of an antiferromagnetic dilute Cr alloy, one usually observes⁴ a small linear increase with pressure, without any hysteresis, for $\Delta W/W_0$ of the c_L propagation mode. For Cr+5 at. % V the slope of the $\Delta W/W_0 - P$ curve for this mode at room temperature is about⁴ 0.01 (GPa)^{-1} and is not expected to change much in the temperature range of the present study.

(2) Well below T_N , $\Delta W/W_0$ for the c_{44} propagation mode of Cr+0.5 at. % Si decreases slightly with increasing pressure with a slope of about -0.02 (GPa)^{-1} up to $40 \times 10^6 \text{ Pa}$, which is an anomalous behavior, as the only previous study¹ done in the ISDW phase of a Cr alloy (Cr+0.3 at. % Ru) gives an increase in $\Delta W/W_0$ with pressure for this propagation mode. Close to T_N and at $T > T_N$, $\Delta W/W_0$ for the c_{44} mode behaves normally with pressure with a small positive slope of about $+0.01 \text{ (GPa)}^{-1}$, similar to the behavior for a paramagnetic Cr alloy.⁴ The behavior of the c' mode is normal, giving a small positive slope, at all temperatures except near T_N where the $\Delta W/W_0 - P$ curve shows signs of the Néel transition, as was also observed for the longitudinal mode in Fig. 1(b). No hysteresis effects were observed for the shear mode $\Delta W/W_0 - P$ curves.

Figure 2(a) shows the temperature dependence of the longitudinal ultrasonic wave velocity for the c_L , propagation mode at different constant pressures of the Cr+0.5 at. % Si alloy single crystal. As usual, T_N is defined at the minimum point on the curve for each pressure in this figure. Figure 2(b) shows the pressure dependence of T_N for this crystal. T_N varies nearly linearly with pressure with $dT_N/dP = -80 \pm 10 \text{ K/GPa}$. This value is to be compared to $dT_N/dP \approx -58 \text{ K/GPa}$ estimated for Cr+0.5 at. % Si from neutron-diffraction data of Endoh, Mizuki, and Ishikawa¹³ (their Fig. 6). It is hard to speculate on possible reasons for the different dT_N/dP results obtained for Cr+0.5 at. % Si in the present ultrasonic investigation and in the previous¹³ neutron-diffraction measurements. One may argue that the deviation may be attributed to different qualities of the crystals used in the two different studies. In both studies the crystals were however grown using the same methods with starting materials of the same purities. Furthermore, the T_N values for Cr+0.5 at. % Si obtained in the two studies compare reasonably well with each other and fit both well in with the known⁷ magnetic phase diagram of Cr-Si alloys. This can safely rule the quality of the crystals out as a possible reason for the observed difference in dT_N/dP . Except the fact that

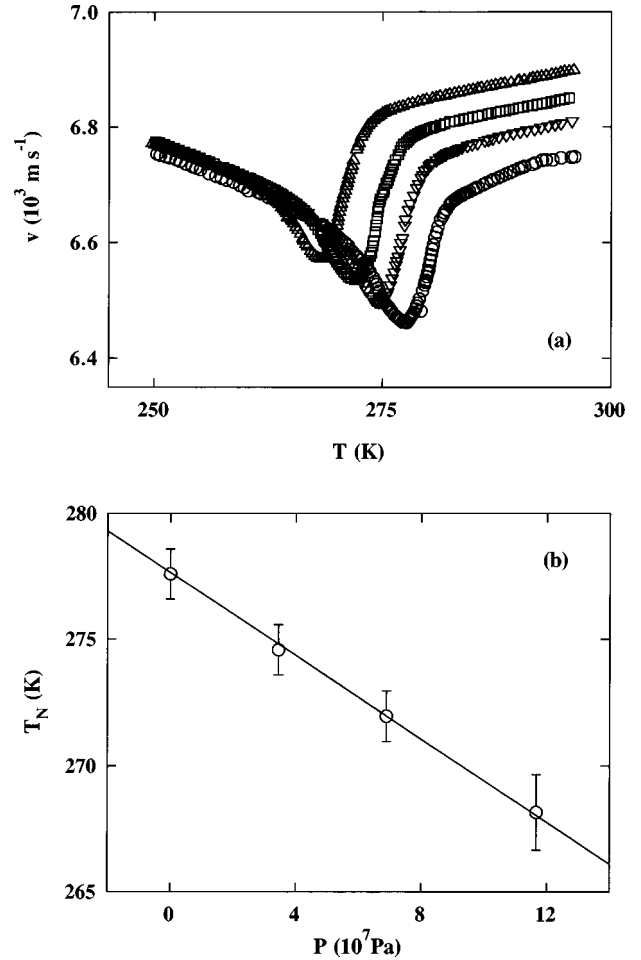


FIG. 2. (a) Longitudinal ultrasonic wave velocity for propagation along [110] as a function of temperature for Cr+0.5 at. % Si. The runs for different constant pressures are denoted by $P = 0 \text{ GPa}$, \circ ; $P = 0.03 \text{ GPa}$, ∇ ; $P = 0.07 \text{ GPa}$, \square ; $P = 0.12 \text{ GPa}$, \triangle . (b) Pressure dependence of T_N for Cr+0.5 at. % Si obtained from the measurements of the effect of hydrostatic pressure on the ultrasonic wave velocities given in (a).

different physical properties were used to follow the pressure dependence of T_N in the two studies, they also differ in the pressure ranges used during measurements. In our study T_N was measured for pressures up to a maximum of 0.12 GPa, while Endoh, Mizuki, and Ishikawa¹³ measured T_N only at two applied pressures, at 0.18 and at 0.35 GPa (which fall outside the pressure range of our experiment), without giving experimental errors. This complicates a proper comparison as it may just be that the $T_N - P$ curve of Cr+0.5 at. % Si shows some curvature, with an initial slope that is slightly larger than the slope at higher pressures. Figure 2(a) clearly shows the marked difference in the pressure dependence of the wave velocity below and above T_N . The velocity is strongly dependent on pressure near and above T_N , while it is nearly pressure independent at $T < T_N$, in agreement with the results in Fig. 1.

In the case of the Cr+1.6 at. % Si crystal the $\Delta W/W_0 - P$ curves behave anomalously in several aspects. Representative examples are shown in Fig. 3 and the results of the measurements are discussed qualitatively below. The interesting features of the $\Delta W/W_0 - P$ measurements of this crystal at different constant temperatures are:

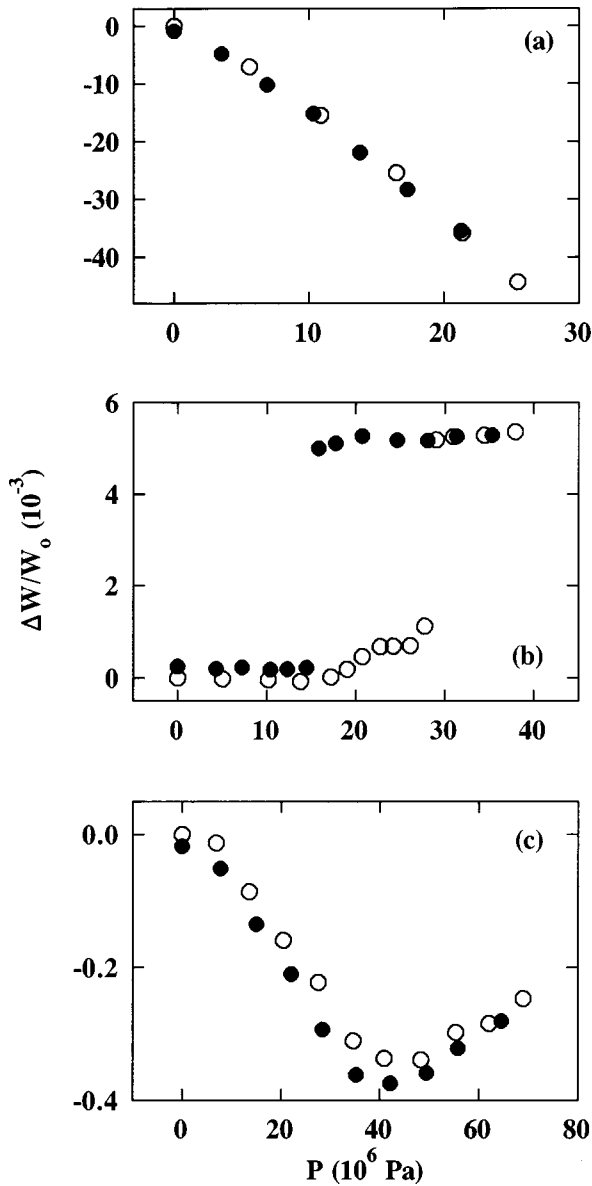


FIG. 3. Pressure dependence of the relative change in natural velocity, $\Delta W/W_0$, of Cr+1.6 at. % Si for (a) the c_L mode at $T = 241$ K, (b) the c_{44} mode at $T = 241$ K and (c) the c' mode at 260 K. In (a), (b), and (c) \circ represents the results for increasing and \bullet for decreasing pressure. Note the different pressure scales.

(1) Below T_N , in the case of the CSDW phase, $\Delta W/W_0$ for the c_L propagation mode of Cr+1.6 at. % Si behaves unusually with pressure; it decreases sharply with increasing pressure [for example, Fig. 3(a)], in contrast with the behavior of a paramagnetic Cr+5 at. % V alloy for which $\Delta W/W_0$ for the c_L mode increases only slightly with pressure.⁴ The anomalous behavior below T_N is due to the CSDW and was previously also observed in the CSDW phases of Cr-Ru (Ref. 1) and Cr-Al (Ref. 3) alloys. When compared to Cr+5 at. % V the behavior of $\Delta W/W_0$ for the c_L mode at $T > T_N$ is also anomalous. Although $\Delta W/W_0$ was observed to increase with pressure at $T > T_N$, as expected for the paramagnetic Cr alloy, the rate of increase is very large, about 60 times larger close to T_N than for Cr+5 at. % V.⁴ The rate decreases, tending to the paramagnetic value of Cr+5 at. % V when the temperature is increased to well above T_N .

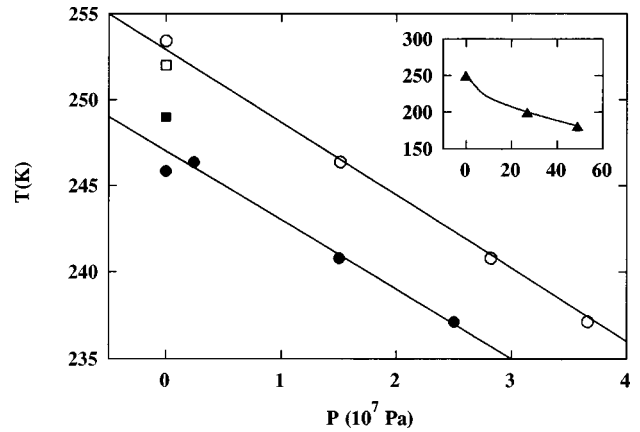


FIG. 4. Pressure dependence of T_N for Cr+1.6 at. % Si obtained from measurements of the pressure dependence of the relative change in natural velocity, $\Delta W/W_0$, for the c_{44} mode of Cr+1.6 at. % Si at different constant temperatures. \circ denotes data obtained during increasing and \bullet during decreasing pressure runs. \square denotes the data obtained at atmospheric pressure for increasing and \blacksquare for decreasing temperature runs reported by Anderson, Alberts, and Smit (Ref. 8). The inset shows the results obtained by Fernandez-Baca *et al.* (Ref. 14).

(2) At $T > T_N$ and $T < T_N$, $\Delta W/W_0$ for the c_{44} shear mode of Cr+1.6 at. % Si increases slowly with increasing pressure, similarly to the observation for paramagnetic Cr+5 at. % V.⁴ For $T < T_N$ but close to T_N [Fig. 3(b)], the $\Delta W/W_0 - P$ curve for the c_{44} mode behaves anomalously. There appears a transition, both during increasing and decreasing pressure runs, that is accompanied by hysteresis effects and by a near discontinuity at a certain critical pressure. We interpret the discontinuity to occur at the first-order CSDW-P Néel transition on applying the critical pressure. A similar behavior was observed for the c' mode. $\Delta W/W_0$ for the c_L mode could not be measured to high enough pressures for the pressure-induced transition to occur. The reason being very high ultrasonic attenuation for this mode at the CSDW-P transition. Below T_N the $\Delta W/W_0 - P$ curve for the c' mode behaves normally with a small positive slope. At $T > T_N$ it however behaves unusually in that $\Delta W/W_0$ for this mode at first decreases with increasing pressure and then increases again [Fig. 3(c)]. This behavior was found at all temperatures studied above T_N and the reason for this behavior is presently unknown. The pressure-induced Néel transition was studied in detail for the c_{44} propagation mode at constant temperatures of 237, 241, and 246 K. An example of the measurements is shown in Fig. 3(b). The critical pressure for the transition, both for increasing and decreasing pressures, is taken at the midpoint of the sharp rise, or sharp drop, respectively, for each temperature [see the example of Fig. 3(b)]. Figure 4 shows the pressure dependence of T_N for Cr+1.6 at. % Si obtained from the results. T_N decreases linearly with pressure, giving dT_N/dP (increasing pressure) = $-(410 \pm 10)$ K/GPa and dT_N/dP (decreasing pressure) = $-(440 \pm 30)$ K/GPa. Neutron-diffraction experiments were recently¹⁴ done on a Cr+1.6 at. % Si crystal, cut from the same crystal boule as the present one, during increasing temperature runs at different constant pressures up to 0.69 GPa. T_N obtained from the neutron-diffraction experiments decreases nonlinearly in the pressure range as

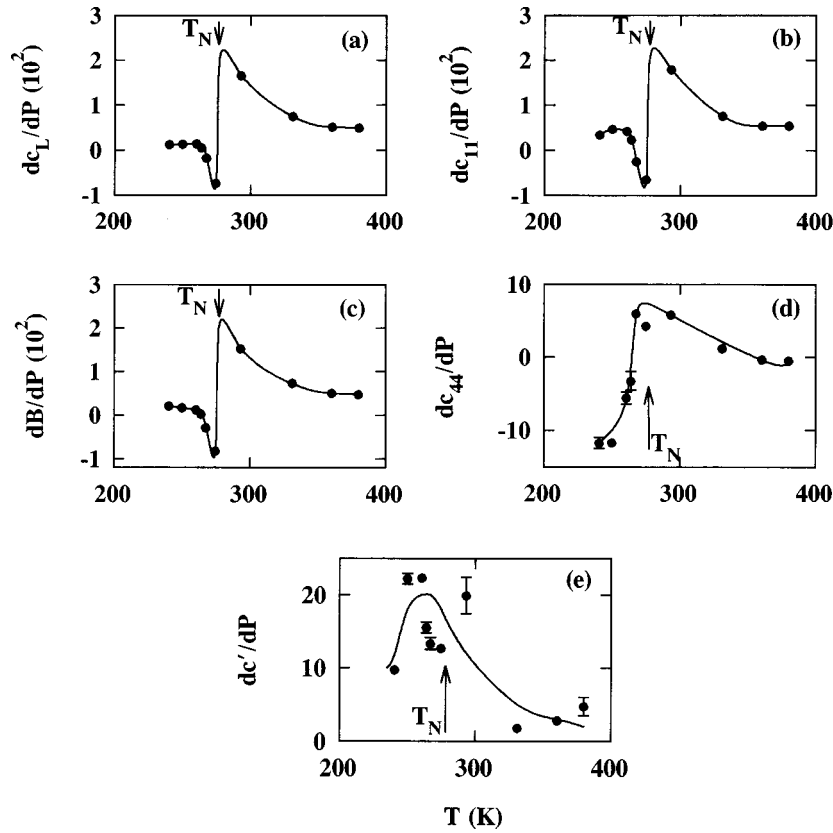


FIG. 5. The pressure dependences of (a) dc_L/dP , (b) dc_{11}/dP , (c) dB/dP , (d) dc_{44}/dP , and (e) dc'/dP for Cr+0.5 at. % Si. The smooth curves through the data points are guides to the eye. Error bars are shown. For points without an error bar the error is within the size of the point itself.

shown in the inset of Fig. 4. The present experiments were done only up to 0.04 GPa and the slope of the T_N - P curves obtained in our study fits well in with the initial slope of the curve in the inset. dT_N/dP of the Cr+1.6 at. % Si crystal is relatively large when compared with other Cr alloys with a CSDW-P Néel transition.⁷ Similar large values for dT_N/dP were however previously also reported by Jayaraman *et al.*¹⁵ for Cr+1.38 at. % Si and Cr+1.85 at. % Si and by Hochheimer and Münch¹⁶ for Cr+1.85 at. % Si.

The Clausius-Clapeyron equation¹⁷ for first-order phase transitions can be used to calculate the latent heat, ΔL , associated with the first-order CSDW-P Néel transition of Cr+1.6 at. % Si by using our measurements for dT_N/dP and previous⁸ measurements for the discontinuity in the volume ($\Delta V/V \approx 4 \times 10^{-4}$) at the first-order Néel transition of this crystal. The calculated value is $\Delta L = 5.0 \text{ J mol}^{-1}$. This value compares well with direct measurements of $\Delta L = 4.2 \text{ J mol}^{-1}$ for a Cr+1.67 at. % Si alloy by Benediktsson *et al.*¹⁸

Figures 5 and 6 show the temperature dependences of $(dc_L/dP)_{P=0}$, $(dc_{11}/dP)_{P=0}$, $(dB/dP)_{P=0}$, $(dc_{44}/dP)_{P=0}$, and $(dc'/dP)_{P=0}$ for Cr+0.5 at. % Si and Cr+1.6 at. % Si, respectively, calculated from the initial slopes of the $\Delta W/W_0$ - P curves using Eq. (1). The outstanding features of those two figures are the very sharp rises from largely negative to largely positive values of $(dc_L/dP)_{P=0}$, $(dc_{11}/dP)_{P=0}$, and $(dB/dP)_{P=0}$ near T_N and the peaks in $(dc_{44}/dP)_{P=0}$ and $(dc'/dP)_{P=0}$ near this temperature for both crystals. The peaks in $(dc_{44}/dP)_{P=0}$ and

$(dc'/dP)_{P=0}$, for Cr+0.5 at. % Si are broad compared to those for Cr+1.6 at. % Si. The data for $(dc'/dP)_{P=0}$ for Cr+0.5 at. % Si show some scattering (Fig. 5). The trend is however for a peak near T_N , as shown by the curve drawn as a guide to the eye in the panel for $(dc'/dP)_{P=0}$ in Fig. 5. The general behavior of the temperature dependence of the pressure derivatives of the elastic constants of both the Cr+0.5 at. % Si and Cr+1.6 at. % Si crystals is very similar to that previously observed³ for a Cr+3.5 at. % Al crystal. The behavior for the three crystals differs however in one important aspect. The sharp increases of about 2000 observed in $(dc_L/dP)_{P=0}$, $(dc_{11}/dP)_{P=0}$, and $(dB/dP)_{P=0}$ at the first-order CSDW-P Néel transition of Cr+1.6 at. % Si is much larger than that (about 300) observed at the second-order ISDW-P Néel transition of Cr+0.5 at. % Si and that³ (about 500) observed at the second-order CSDW-P Néel transition of Cr+3.5 at. % Al. Large increases in the pressure derivatives of the longitudinal elastic constants in going through a CSDW-P Néel transition were previously¹ also observed for Cr+0.3 at. % Ru crystal for which these changes are about 700.

The volume of SDW antiferromagnets like Cr and its alloys increases when the material is cooled through T_N from the paramagnetic to the SDW phase.⁷ One then expects^{2,3} the latter phase to be more sensitive to the effects of the applied pressure than the former. This may partly account^{2,3} for much larger values of $|dc_L/dP|$, $|dc_{11}/dP|$, and $|dB/dP|$ observed in the present study for the volume-dependent lon-

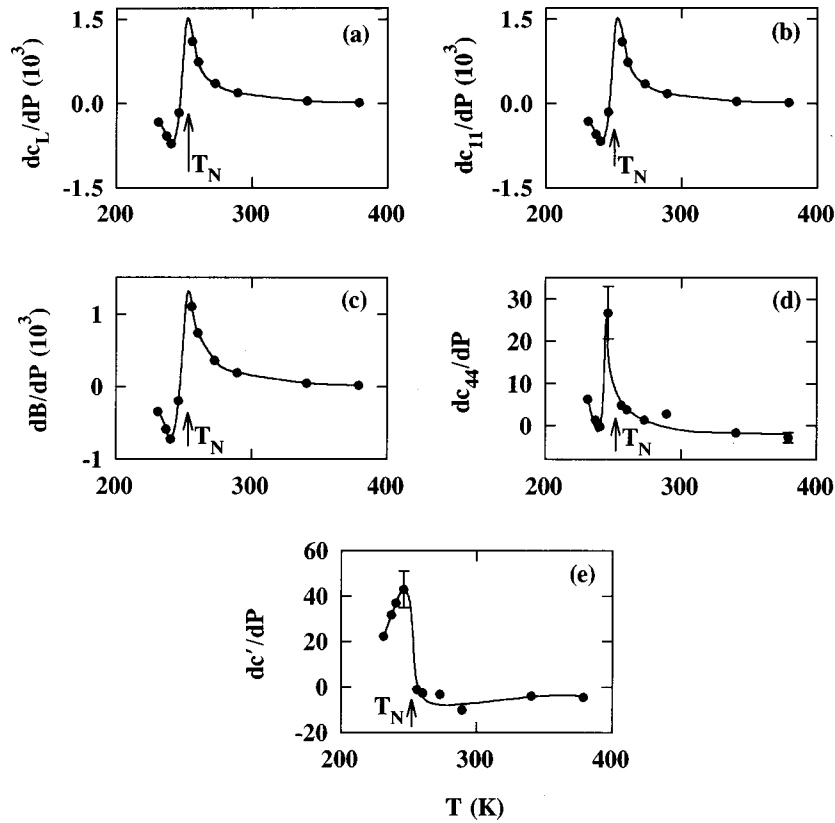


FIG. 6. The pressure dependences of (a) dc_L/dP , (b) dc_{11}/dP , (c) dB/dP , (d) dc_{44}/dP , and (e) dc'/dP for Cr+1.6 at. % Si. The smooth curves through the data points are guides to the eye. Error bars are shown. For points without an error bar the error is within the size of the point itself.

gitudinal modes in the SDW phase just below T_N than in the paramagnetic phase well above T_N . Previous measurements⁸ show that the volume increase through the first-order CSDW-P transition of Cr+1.6 at. % Si is much larger than that through the second-order ISDW-P transition of Cr+0.5 at. % Si, accounting in part for the larger absolute values of the pressure derivatives of the longitudinal mode elastic constants in the SDW phase of the former crystal than of the latter.

Large negative dc_L/dP , dc_{11}/dP , and dB/dP observed in the ISDW phase of Cr+0.5 at. % Si and in the CSDW phase of Cr+1.6 at. % Si were previously also observed in the CSDW phase of Cr+3.5 at. % Al and in both the ISDW and CSDW phases of Cr+0.3 at. % Ru and are due to large magnetoelastic interactions in the crystals. The magnetoelastic interactions seem to be much larger in the CSDW Cr-Si alloy than in the ISDW one.

IV. GRÜNEISEN PARAMETERS OF Cr+0.5 at. % Si AND Cr+1.6 at. % Si ALLOY SINGLE CRYSTALS

The volume dependence of the long-wavelength acoustic-mode frequency ω_p in a phonon branch p , is expressed by a mode Grüneisen parameter defined by

$$\gamma_p = - \left(\frac{\partial \ln \omega_p}{\partial \ln V} \right)_T. \quad (2)$$

γ_p is obtained from the measurements of the elastic constants and their pressure dependences using equations given

by Brugger and Fritz¹⁹ for the anisotropic continuum model. These type of calculations, as applied to Cr+0.3 at. % Ru and Cr+3.5 at. % Al, were described in some detail previously.^{2,3} γ_p was calculated along those lines at each constant temperature as a function of mode propagation direction for both the Cr+0.5 at. % Si and Cr+1.6 at. % Si single crystals. Figure 7 shows a typical example, that for Cr+1.6 at. % Si, at temperatures below, close to and above T_N . The temperature dependence of the acoustic-mode Grüneisen parameters for all three propagation modes of Cr+0.5 at. % Si and Cr+1.6 at. % Si is shown, respectively, in Figs. 8 and 9. Relatively large anisotropy for the different mode γ_p 's are observed at temperatures close to T_N of the Cr+1.6 at. % Si crystal (Fig. 7). These anisotropy effects are relatively small at other temperatures (Fig. 7). For this crystal the longitudinal-mode γ_p is largely negative at all $T < T_N$, jumping to largely positive values at T_N (Fig. 9). This behavior is similar to the previous observation for Cr+3.5 at. % Al (Ref. 3) and Cr+0.3 at. % Ru (Ref. 1). The absolute values of the longitudinal-mode γ_p below and above T_N are, however, much larger for Cr+1.6 at. % Si than for Cr+3.5 at. % Al and Cr+0.3 at. % Ru. For Cr+1.6 at. % Si this mode γ_p reaches values of up to -150 below T_N and up to $+300$ above T_N compared to -20 and $+120$ for Cr+3.5 at. % Al (Ref. 3) and -100 to $+5$ for Cr+0.3 at. % Ru (Ref. 1). For Cr+0.5 at. % Si relatively large anisotropy was also observed in the shear mode γ_p , not only close to T_N but at all temperatures below T_N . This anisotropy at $T < T_N$ is roughly four times smaller than the

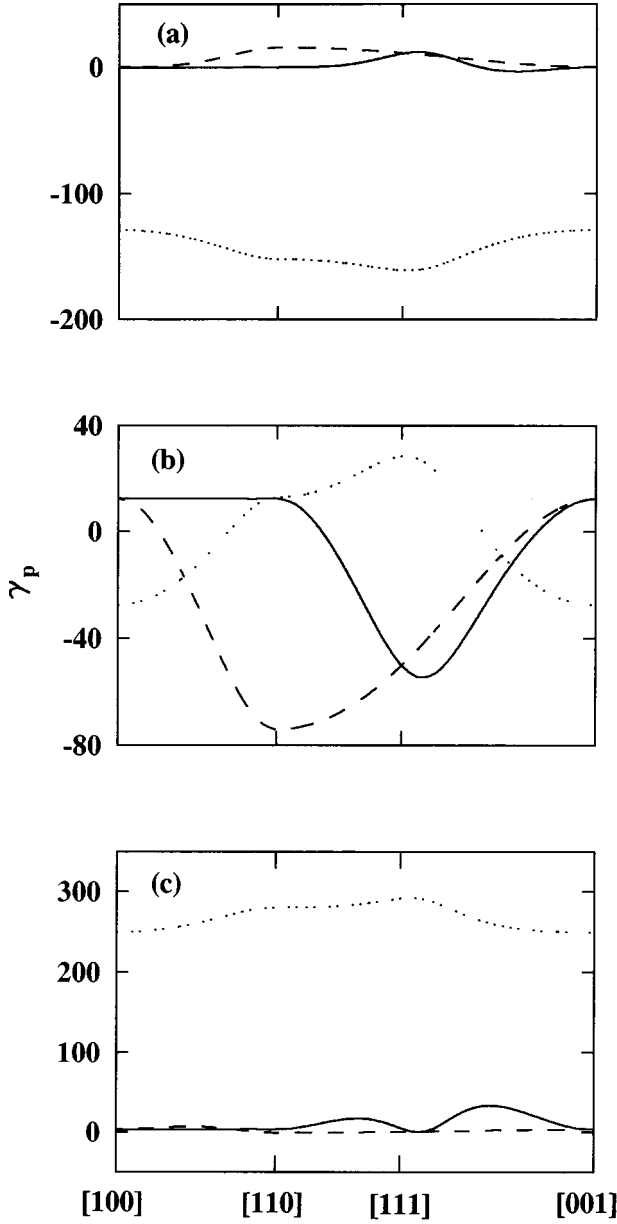


FIG. 7. Long-wavelength acoustic-mode Grüneisen parameters, γ_p , for Cr+1.6 at. % Si as a function of mode propagation direction at (a) $T=241$ K, (b) $T=246$ K and (c) $T=256$ K. The longitudinal acoustic mode γ_p is represented in (a), (b), and (c) by the dotted curve, while the solid and broken curves represent the shear acoustic mode γ_p 's in all three cases.

anisotropy observed for Cr+1.6 at. % Si close to T_N in Fig. 7(b). It becomes a little smaller as the temperature is increased to above T_N . Furthermore, the longitudinal-mode γ_p for Cr+0.5 at. % Si is positive well below T_N , becomes negative close to T_N and switches to relatively large positive values just above T_N . Also of interest is the negative shear-mode γ_p values that were observed in the [100] and [001] directions of Cr+0.5 at. % Si at temperatures below T_N and its change to positive values for these directions close to and above T_N . A similar effect was observed for Cr+1.6 at. % Si, but in this case the shear mode γ_p is negative along the [110] and [111] directions and only at temperatures close to T_N (Fig. 7). The shear-mode γ_p 's are affected differently by

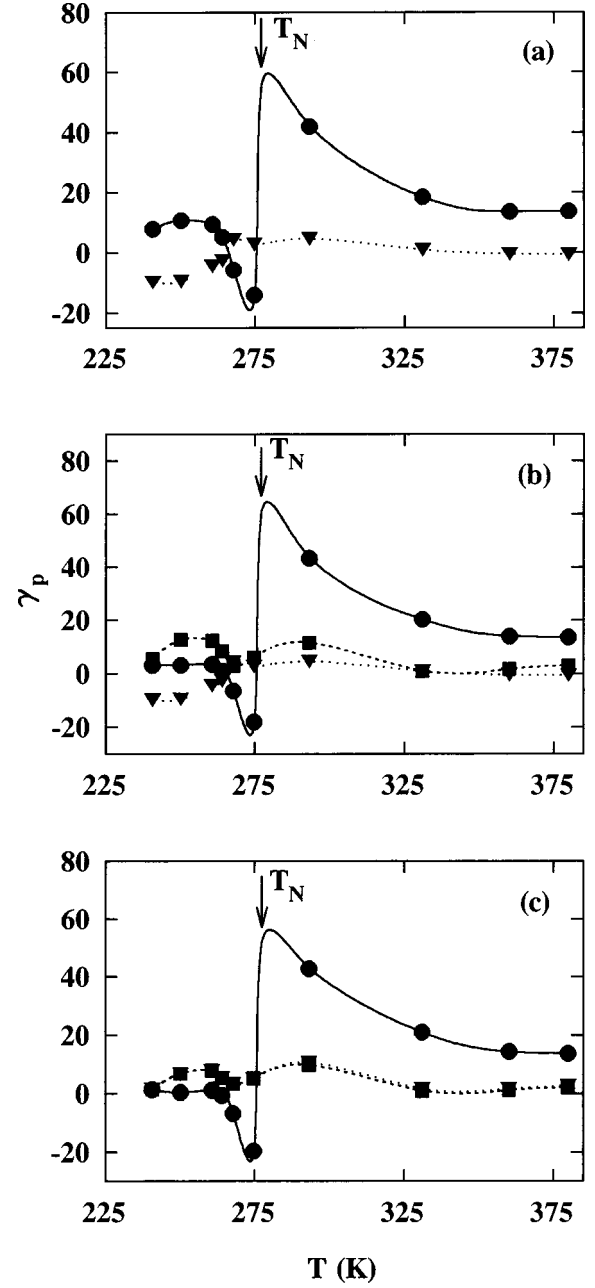


FIG. 8. Long-wavelength acoustic-mode Grüneisen parameters, γ_p , for Cr+0.5 at. % Si as a function of temperature for mode propagations along (a) [100], (b) [110], and (c) [111]. The longitudinal mode γ_p is represented in (a), (b), and (c) by \bullet , and the shear mode γ_p 's by \blacksquare and \blacktriangledown in all three cases. The curves through the data points are guides to the eye.

the Néel transition than the longitudinal-mode γ_p for both Cr-Si crystals (Figs. 8 and 9). For both it is mainly the longitudinal-mode constant that is affected. Shear-mode effects are much smaller, particularly for Cr+1.6 at. % Si. The contribution of the acoustic modes at the Brillouin-zone center to the anharmonicity is given by the mean long-wavelength acoustic-mode Grüneisen parameter

$$\bar{\gamma}^{el} = \frac{\sum_{p=1}^3 \int_{\Omega} \gamma_p d\Omega}{3 \int_{\Omega} d\Omega}, \quad (3)$$

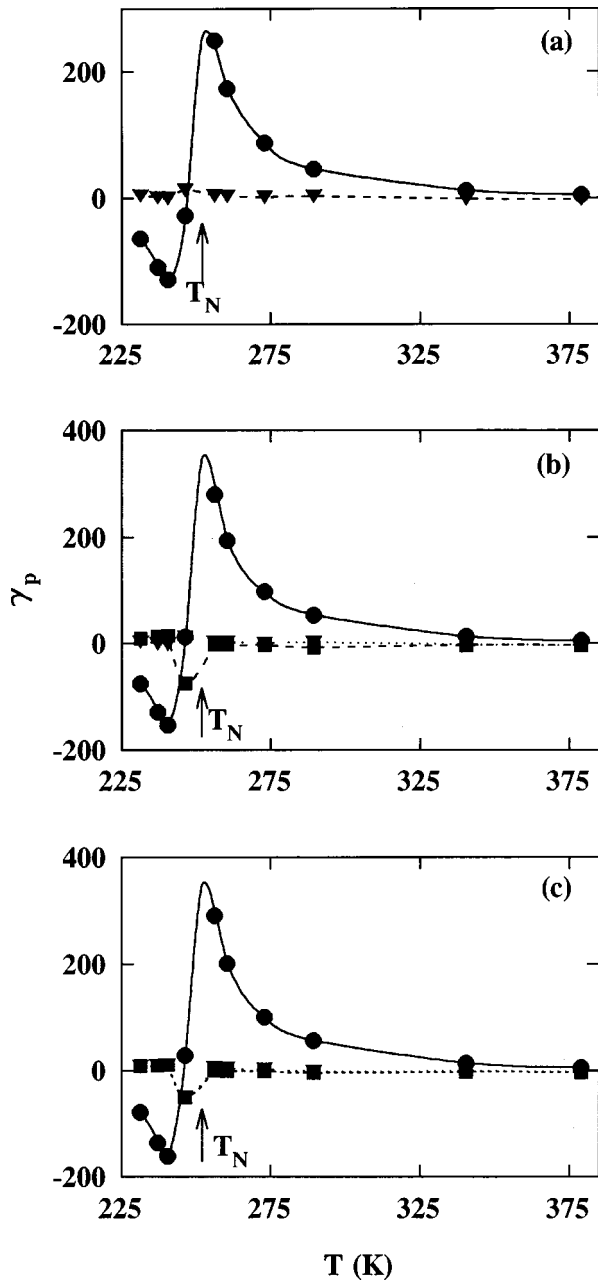


FIG. 9. Long-wavelength acoustic-mode Grüneisen parameters, γ_p , for Cr+1.6 at. % Si as a function of temperature for mode propagations along (a) [100], (b) [110], and (c) [111]. The longitudinal mode γ_p is represented in (a), (b), and (c) by \bullet , and the shear mode γ_p 's by \blacksquare and \blacktriangledown in all three cases. The curves through the data points are guides to the eye.

where the integration in Eq. (3) is over the whole of space Ω . Figures 10(a) and 10(b) show, respectively, $\bar{\gamma}^{el}$ calculated from Eq. (3) as a function of temperature for the Cr+0.5 at. % Si and Cr+1.6 at. % Si single crystals. The large peak in $\bar{\gamma}^{el}$ observed close to T_N indicates large mean vibrational anharmonicity of long-wavelength acoustic phonons near the Néel temperatures of both crystals. The anharmonicity is however about four times stronger for the first-order CSDW-P Néel transition of Cr+1.6 at. % Si than for the second-order ISDW-P transition of Cr+0.5 at. % Si. The magnetoelastic interactions lead to the longitudinal-mode softening in the ISDW phase of Cr+0.5 at. % Si and

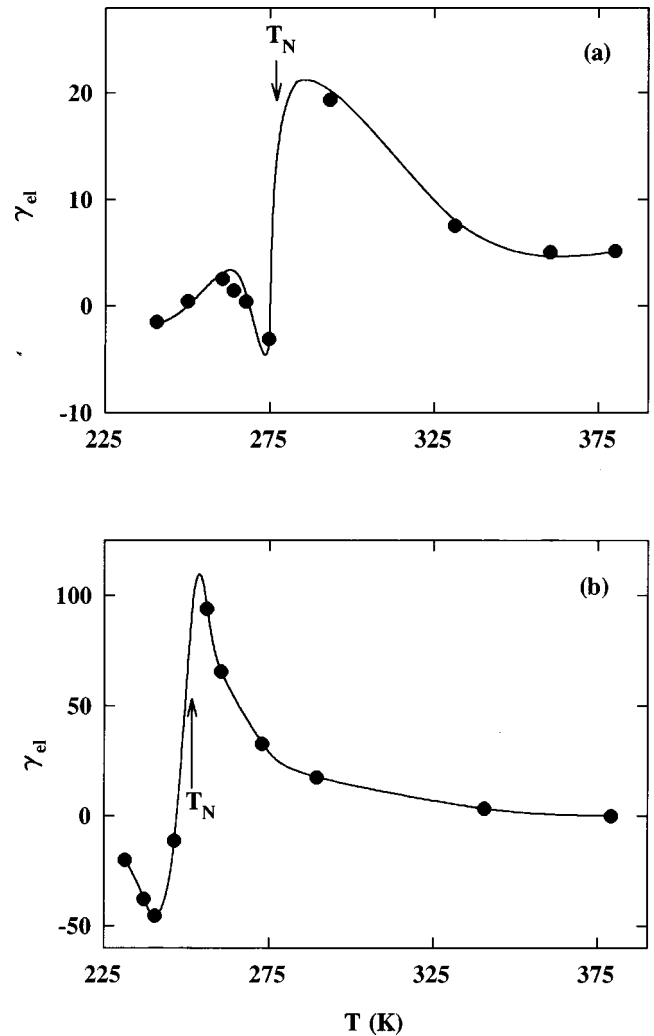


FIG. 10. The temperature dependence of the mean acoustic-mode Grüneisen parameter, $\bar{\gamma}^{el}$, for (a) Cr+0.5 at. % Si and (b) Cr+1.6 at. % Si. The curves through the data points are guides to the eye.

the CSDW phase of Cr+1.6 at. % Si. The softening is much larger, up to ten times larger in the latter case than in the former (Figs. 5 and 6). The unusually large positive $\bar{\gamma}^{el}$ just above T_N [Figs. 10(a) and 10(b)] that decreases with increasing temperature as T goes deeper into the paramagnetic phase, is attributed to strong coupling of the longitudinal phonons to spin fluctuations, similarly to the observation³ in Cr+3.5 at. % Al. This coupling is however much smaller in the case of Cr+0.3 at. % Ru.¹

V. SUMMARY AND CONCLUSION

The main features of the present results on the two Cr-Si crystals compared to previous work on Cr-Al and Cr-Ru crystals, are summarized as follows:

(1) The Néel transition for Cr+0.5 at. % Si is a second-order ISDW-P transition for which anharmonic effects have not been studied before. The behavior of the longitudinal-mode Grüneisen parameters through the ISDW-P transition of this crystal is in general quite similar to that observed^{1,3} for the second-order CSDW-P transitions of Cr+3.5 at. % Al and Cr+0.3 at. % Ru. There are however important differ-

ences. Longitudinal-mode softening due to the SDW in the ISDW phase of Cr+0.5 at. % Si, occurs only in a small temperature interval of less than about 15 K very close to T_N and is absent at lower temperatures. On the other hand, this softening exist for Cr+3.5 at. % Al, (Ref. 3) and Cr+0.3 at. % Ru (Ref. 1) down to temperatures well into their CSDW phases. The longitudinal-mode softening in all three crystals is largest just below their Néel temperatures, being of about similar magnitudes for the ISDW phase of Cr+0.5 at. % Si and the CSDW phase of Cr+3.5 at. % Al,³ but nearly five times larger in the CSDW phase of Cr+0.3 at. % Ru.¹ There is very large longitudinal-mode stiffening for the Cr+0.5 at. % Si and Cr+3.5 at. % Al. (Ref. 3) crystals just above T_N , being largest for Cr+3.5 at. % Al and nearly three times smaller for Cr+0.5 at. % Si. This stiffening effect is negligibly small in the case of Cr+0.3 at. % Ru.¹ Shear-mode softening, comparable to that of the longitudinal modes, occurs in the ISDW phase of Cr+0.5 at. % Si to temperatures much lower than the longitudinal-mode softening. Shear-mode softening was previously also observed^{1,2} in the CSDW phase of Cr+0.3 at. % Ru but in this case its magnitude is much smaller than the longitudinal-mode softening. Shear-mode softening is negligible in the CSDW phase of Cr+3.5 at. % Al.³

(2) The Néel transition for Cr+1.6 at. % Si is a first-order CSDW-P transition, not studied before for anharmonic effects. The longitudinal-mode Grüneisen parameters through this transition behave very similar to that for the second-

order CSDW-P transition of Cr+3.5 at. % Al.³ There is large longitudinal-mode softening in the CSDW phases as well as large stiffening of this mode just above T_N for both. The main influence of the first-order CSDW-P transition (Cr+1.6 at. % Si) on these is that both the stiffening and softening effects are much larger, respectively, nearly two times and ten times larger, than for the second-order CSDW-P transition (Cr+3.5 at. % Al). The discontinuity in volume ($\Delta V/V \approx 4 \times 10^{-4}$) occurring at the first-order CSDW-P transition in Cr+1.6 at. % Si may partly be responsible for this difference.

In conclusion, the role of magnetoelastic effects in the acoustic-mode vibrational anharmonicity near the Néel transition of Cr+0.5 at. % Si and Cr+1.6 at. % Si alloy single crystals have been studied through high-pressure elastic constant measurements. The interaction between the SDW and the long-wavelength longitudinal acoustic phonons plays a dominant role in the elastic behavior of both crystals through the Néel transition. Shear-mode effects are relatively weak. The anharmonicity through the Néel temperature of dilute Cr alloys seems to behave in several aspects very similarly, whether it is through a first order CSDW-P, a second-order CSDW-P or a second-order ISDW-P transition.

ACKNOWLEDGMENT

We are grateful to the South African FRD for financial support.

¹M. Cankurtaran, G. A. Saunders, H. A. A. Sidek, Q. Wang, and H. L. Alberts, *Phys. Rev. B* **53**, 11 408 (1996).

²M. Cankurtaran, G. A. Saunders, Q. Wang, P. J. Ford, and H. L. Alberts, *Phys. Rev. B* **46**, 14 370 (1992).

³H. L. Alberts and P. Smit, *Phys. Rev. B* **51**, 15 146 (1995).

⁴M. Cankurtaran, G. A. Saunders, H. A. A. Sidek, and H. L. Alberts, *Philos. Mag. B* **74**, 349 (1996).

⁵T. Suzuki, *J. Phys. Soc. Jpn.* **41**, 1187 (1976).

⁶T. Suzuki, *J. Phys. Soc. Jpn.* **43**, 869 (1977).

⁷E. Fawcett, H. L. Alberts, V. Yu Galkin, D. R. Noakes, and J. V. Yakhmi, *Rev. Mod. Phys.* **66**, 25 (1994).

⁸R. A. Anderson, H. L. Alberts, and P. Smit, *J. Phys., Condens. Matter* **5**, 1733 (1993).

⁹E. P. Papadakis, in *Physical Acoustics*, edited by W. P. Mason and R. N. Thurston (Academic, New York, 1976), Vol. XII.

¹⁰E. Kittinger, *Ultrasonics* **15**, 30 (1977).

¹¹R. N. Thurston, *Proc. IEEE* **53**, 1320 (1965).

¹²H. L. Alberts, *J. Phys. Condens. Matter* **2**, 9707 (1990).

¹³Y. Endoh, J. Mizuki, and Y. Ishikawa, *J. Phys. Soc. Jpn.* **51**, 2826 (1982).

¹⁴J. A. Fernandez-Baca, E. Fawcett, H. L. Alberts, V. Yu Galkin, and Y. Endoh, *J. Appl. Phys.* **81**, 3877 (1997).

¹⁵A. Jayaraman, R. G. Maines, K. V. Rao, and S. Araj, *Phys. Rev. Lett.* **37**, 926 (1976).

¹⁶H. D. Hochheimer and R. Münch, *Philos. Mag. B* **63**, 979 (1991).

¹⁷F. Reif, *Fundamentals of Statistical and Thermal Physics* (McGraw-Hill, Singapore, 1987).

¹⁸G. Benediktsson, L. Hedman, H. U. Åström, and K. V. Rao, *J. Phys. F* **12**, 1439 (1982).

¹⁹K. Brugger and T. C. Fritz, *Phys. Rev.* **157**, 524 (1967).